

CHARACTERIZATION OF DEFECT MODES IN ONE-DIMENSIONAL TERNARY METALLO-DIELECTRIC NANOLAYERED PHOTONIC CRYSTAL

A. Gharaati* and H. Azarshab

Department of Physics, Payame Noor University, P. O. Box 19395-4697, Tehran, I. R. of Iran

Abstract—We investigate the characterization of defect modes in one-dimensional ternary symmetric metallo-dielectric photonic crystal (1DTSMDPC) band-gap structures. We consider the defect modes for symmetric model with respect to the defect layer. We demonstrate reflectance with respect to the wavelength and its dependence on different thicknesses and indices of refraction of dielectric defect layer, angle of incidence and number of periods for both transverse electric (*TE*) and transverse magnetic (*TM*) waves. Also, we investigate properties of the defect modes for different metals. Our findings show that the photonic crystal (PC) with defect layer, made of two dielectrics and one metallic material, leads to different band-gap structures with respect to one dielectric and one metallic layer. There is at least one defect mode when we use dielectric or metallic defect layer in symmetric structure. And, the number of defect modes will be increased by the enhancement of refractive index and thickness of dielectric defect layer.

1. INTRODUCTION

In recent years, advances in photonic crystal (PC) technology have attracted a great deal of attention. The main attraction of PCs is the existence of forbidden band gaps in their transmission spectra. PCs are regular arrays of materials with different refractive indices [1, 2]. The simplest possible PC consists of alternating layers of material with different dielectric constants. PCs can control the propagation and localization of light, and have shown very promising applications as functional photonic devices [3, 4]. Actually, according to the number of layers in each period, PCs can be classified into categories like

Received 14 October 2011, Accepted 5 December 2011, Scheduled 12 December 2011

* Corresponding author: Abdolrasoul Gharaati (Agharaati@pnu.ac.ir).

binary, ternary and so on. Binary PC includes two layers in each period; ternary PC contains three layers in each period and so on. Finally, these periods are repeated several times to form PCs [5]. 1D PCs can be dielectric with negative index of refraction in which optical properties change in one direction, while in two other directions, the structure is uniform [6]. The simplest PC is unidimensional and corresponds to a Bragg reflector. A two-dimensional PC can be a set of parallel identical cylinders (dielectric or metallic rods in a dielectric material) periodically arranged in homogeneous medium. A three-dimensional crystal can be, for instance, a set of identical spheres periodically arranged. But many other patterns have also been tested [7]. A one-dimensional ternary symmetric metallo-dielectric photonic crystal (1DTSMDPC) is a periodic structure consisting of dielectric and metal elements with different refractive indices. There are some advantages in using metals in PCs such as decreased size, simpler fabrication, and lower costs. 1DTSMDPC has wider band gaps as compared with one-dimensional binary symmetric metallo-dielectric photonic crystal (1DBSMDPC) and the speed of enhancement of defect modes with increasing thickness and index of refraction of dielectric defect layer in 1DTSMDPC is more than 1DBSMDPC. Because 1D PCs have easy fabrication, they have many applications such as multilayer's coatings [8], Bragg reflectors [9], narrow band filters [10], and fibers [11]. Besides, there are a lot of researches in using metals in recent years [12–16]. Photonic band gap (PBG) is in the ranges of frequency in which light cannot propagate through the PC. Moreover, if we enter a disorder into the regular dielectric structure of the PC, we will obtain mid gap modes whose eigenfunctions are localized around the disorder. These modes are called localized defect modes [1].

There are some analytical techniques to investigate the defect mode wavelength in 1D PCs such as transverse matrix method (TMM) [17, 18], plane wave expansion (PWE) [19, 20], etc. We have used TMM to calculate the transmission and reflection coefficients of incident electromagnetic waves. In a defective PC made of dielectric and metallic layer, we calculate its dependence on the index of refraction, thickness, number of unit cells, and angle of incidence for symmetric geometries.

In this study, using TMM, we develop an analytical method for calculating the defect mode wavelength. We apply this method to a 1D PC consisting of periodically dielectric-metal-dielectric with dielectric and metallic defect layer for both TE and TM waves. We show that the number of defect modes will increase by the enhancement of defect layer thickness and refractive index. The structure of symmetric defective PC is made by the defect layer D , which is denoted as

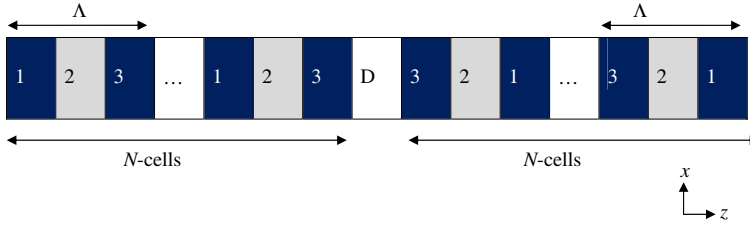


Figure 1. The structure of 1D TSM DPCs.

$A/(n_1n_2n_3)^N D(n_3n_2n_1)^N/A$, where A means the usual air, N is the number of periods and n_1, n_2 and n_3 are the refractive indices of dielectric, metal and dielectric layers, respectively. This structure is depicted in Figure 1.

2. THEORETICAL ANALYSIS

A 1D TSM DPC with a structure of $A/(n_1n_2n_3)^N D(n_3n_2n_1)^N/A$ is made of a dielectric or a metallic defect layer with thickness d_{def} sandwiched by two N -cells in which it puts in air ($n_A = 1$), and each cell make up with a metallic layer 2 that is sandwiched by two dielectric layer 1 and 3. The thicknesses of the layers are denoted by d_1, d_2 and d_3 , respectively, as shown in Figure 1. The Drude model [21, 22] is invoked to characterize the wavelength dependence of metallic layer. We assume that the temporal part of the field to be $e^{-i\omega t}$. So metal permittivity in Drude model is

$$\epsilon_2(\omega) = 1 - \frac{\omega_p^2}{\omega^2 - i\gamma\omega}, \tag{1}$$

where ω_p and γ are the plasma frequency and damping coefficient, respectively. We have taken the lossless system. The optical properties of materials that are transparent to electromagnetic (EM) waves can be characterized by an index of refraction and is given by $n = \sqrt{\epsilon\mu}$, where ϵ is the relative dielectric permittivity and μ is the relative permeability of the medium which equals 1 for metals [23]. Then metal refractive index is given by $n_2 = \sqrt{\epsilon_2}$.

In Figure 2, we show a one layer with the components of the electric and magnetic fields of the incident, reflected, and transmitted wave [17, 24].

In this figure, we suppose a layer with index of refraction n_1 put on air, as shown in Figure 2. The incident beam undergoes an external reflection at the first interface (a) and the transmitted beam undergoes an internal reflection and transmission at the second interface (b).

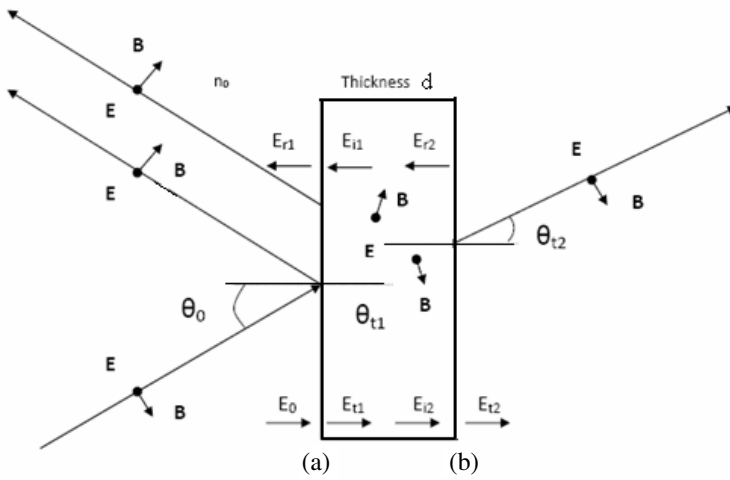


Figure 2. A schematic of one layer of 1DTSMDPC.

According to the boundary conditions, the tangential components of the resultant electric and magnetic fields are continuous across the interface,

$$\begin{aligned} E_a &= E_0 + E_{r1} = E_{t1} + E_{i1}, \\ E_b &= E_{i2} + E_{r2} = E_{t2} \end{aligned} \quad (2)$$

and

$$\begin{aligned} B_a &= B_0 \cos \theta_0 - B_{r1} \cos \theta_0 = B_{t1} \cos \theta_{t1} - B_{i1} \cos \theta_{t1}, \\ B_b &= B_{i2} \cos \theta_{t1} - B_{r2} \cos \theta_{t1} = B_{t2} \cos \theta_{t2} \end{aligned} \quad (3)$$

where the magnetic field has tangential and perpendicular components. Using Maxwell equations, we have the relation $k_0 = \omega \sqrt{\mu_0 \epsilon_0}$, where it is the wave vector in the air, $B = n \sqrt{\mu_0 \epsilon_0} E$, $p_\ell = n_\ell \cos \theta_\ell$, and $\beta_\ell = k_0 n_\ell d_\ell \cos \theta_\ell$, where $\ell = 1, 2$, and 3. So, the electric fields become: $E_{i2} = E_{t1} e^{-i\beta_1}$ and $E_{i1} = E_{r2} e^{-i\beta_1}$ and when included in the boundary conditions, E_{t1} and E_{i1} can be solved in terms of E_a and B_b as:

$$\begin{aligned} E_{i1} &= \frac{(p_1 E_b + B_b)}{2p_1} e^{-i\beta_1}, \\ E_{t1} &= \frac{(p_1 E_b + B_b)}{2p_1} e^{i\beta_1}. \end{aligned} \quad (4)$$

And finally, substituting the above expressions in the initial fields components and written in matrix form, we have

$$\begin{pmatrix} E_a \\ B_a \end{pmatrix} = \begin{pmatrix} \cos \beta_\ell & \frac{-i}{p_\ell} \sin \beta_\ell \\ -ip_\ell \sin \beta_\ell & \cos \beta_\ell \end{pmatrix} \begin{pmatrix} E_1 \\ B_1 \end{pmatrix} = M_1 \begin{pmatrix} E_1 \\ B_1 \end{pmatrix}. \quad (5)$$

Each layer of PC has its own transfer matrix, and the overall transfer matrix of the system is the product of individual transfer matrices. So the characteristics matrix $M(\Lambda)$ for a single period is expressed as [25–27]

$$M(\Lambda) = \begin{bmatrix} M_{11} & M_{12} \\ M_{21} & M_{22} \end{bmatrix} = \prod_{\ell=1}^3 \begin{bmatrix} \cos \beta_{\ell} & \frac{1}{ip_{\ell}} \sin \beta_{\ell} \\ -ip_{\ell} \sin \beta_{\ell} & \cos \beta_{\ell} \end{bmatrix}. \quad (6)$$

In order to compute the Bloch wave vector, we define the half trace ($\frac{M_{11}+M_{22}}{2}$) as following [16],

$$\begin{aligned} a &= \frac{(M_{11} + M_{22})}{2} = \cos \beta_1 \cos \beta_2 \cos \beta_3 \\ &\quad - \frac{1}{2} \left(\frac{p_1}{p_2} + \frac{p_2}{p_1} \right) \sin \beta_1 \sin \beta_2 \cos \beta_3 \\ &\quad - \frac{1}{2} \left(\frac{p_2}{p_3} + \frac{p_3}{p_2} \right) \cos \beta_1 \sin \beta_2 \sin \beta_3 \\ &\quad - \frac{1}{2} \left(\frac{p_1}{p_3} + \frac{p_3}{p_1} \right) \sin \beta_1 \cos \beta_2 \sin \beta_3, \end{aligned} \quad (7)$$

Then, the total characteristic matrix of the total PC is given by [27],

$$M_T(N\Lambda) = \begin{bmatrix} m_{11} & m_{12} \\ m_{21} & m_{22} \end{bmatrix} = M(\Lambda)^N = \begin{bmatrix} M_{11} & M_{12} \\ M_{21} & M_{22} \end{bmatrix}^N, \quad (8)$$

where the matrix elements of M_T can be obtained in terms of the elements of the single-period matrix, that is

$$m_{11} = M_{11}U_{N-1}(a) - U_{N-2}(a), \quad (9a)$$

$$m_{12} = M_{12}U_{N-1}(a), \quad (9b)$$

$$m_{21} = M_{21}U_{N-1}(a), \quad (9c)$$

$$m_{22} = M_{22}U_{N-1}(a) - U_{N-2}(a), \quad (9d)$$

where U_N is the Chebyshev polynomial of the second kind given by,

$$U_N(a) = \frac{\sin [(N + 1) \cos^{-1}(a)]}{\sqrt{1 - a^2}}. \quad (10)$$

Using of Equations (9), the reflection coefficient, r is given by

$$r = \frac{(m_{11} + m_{12}p_0)p_0 - (m_{21} + m_{22}p_0)}{(m_{11} + m_{12}p_0)p_0 + (m_{21} + m_{22}p_0)}, \quad (11)$$

where $p_0 = n_0 \cos \theta_0$. We can calculate the reflectance $R = |r|^2$.

The above calculations can be used for *TM* wave by substituting $p_\ell = \cos \theta_\ell / n_\ell$ where $\ell = 0, 1, 2$ and 3 . So, the characteristic matrix of left unit cells with the number of periods equal to N is given by [28],

$$M_{cellL} = (M_3 \cdot M_2 \cdot M_1)^N. \quad (12)$$

Then the characteristic matrix for right unit cells with number of periods equal to N in symmetric structure is

$$M_{cellR} = (M_1 \cdot M_2 \cdot M_3)^N. \quad (13)$$

And defect matrix (M_{def}) is given by

$$M_{def} = \begin{bmatrix} \cos \beta_{def} & \frac{1}{ip_{def}} \sin \beta_{def} \\ -ip_{def} \sin \beta_{def} & \cos \beta_{def} \end{bmatrix}. \quad (14)$$

where $\beta_{def} = k_0 n_{def} d_{def} \cos \theta_{def}$, and $p_{def} = n_{def} \cos \theta_{def}$.

Then the characteristics matrix of entire system is expressed as

$$M_{tot} = M_{cellR} \cdot M_{def} \cdot M_{cellL}. \quad (15)$$

3. NUMERICAL RESULTS AND DISCUSSION

In this work, the layers 1 and 3 are ZnSe and Na_3AlF_6 which refractive indices and thicknesses are $n_1 = 2.6$, $d_1 = 90$ nm, $n_3 = 1.34$, and $d_3 = 90$ nm, respectively [22, 29]. The metallic layer is taken to be silver (Ag) with the plasma frequency $\omega_p = 2\pi \times 2.175 \times 10^{15}$ rad/s [30], $d_2 = 10$ nm, and n_2 is calculated with the Drude model of metals Equation (1). The thickness of defect layer is $d_{def} = 120$ nm and its index of refraction is calculated from $n_d \cdot d_{def} = q\lambda_0/4$ with a design wavelength of $\lambda_0 = 1550$ nm in infrared region. We choose the quarter-wavelength stack because of its least loss in optical communication, and q is an optional constant coefficient. The number of periods for right and left cells is equal. The substrate is assumed to be air.

3.1. Defect Modes with Dielectric Defect Layer

In Figure 3, we have plotted the wavelength dependant reflection for the 1DTSMDPC with the structure of $A/(n_1 n_2 n_3)^N D (n_3 n_2 n_1)^N / A$, for normal incidence. We see that there is just one defect mode within the PBG for $d_{def} = 120$ nm and for $q = 1$, $n_d = q\lambda_0/4d_{def} = 3.22$ where it is near the index of refraction of Si. This defect mode is located in 717.5 nm approximately.

In Figure 4, we have plotted the reflectance versus wavelength for normal incidence in a defective 1DTSMDPC. The peak height is decreased by increasing the number of periods. At a much larger N , such as 8 and more, the BG width is decreased in wavelength between

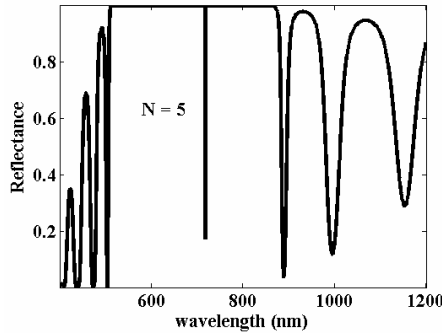


Figure 3. The calculated wavelength-dependant reflectance in 1DTSMDDPC with a dielectric defect layer for normal incident.

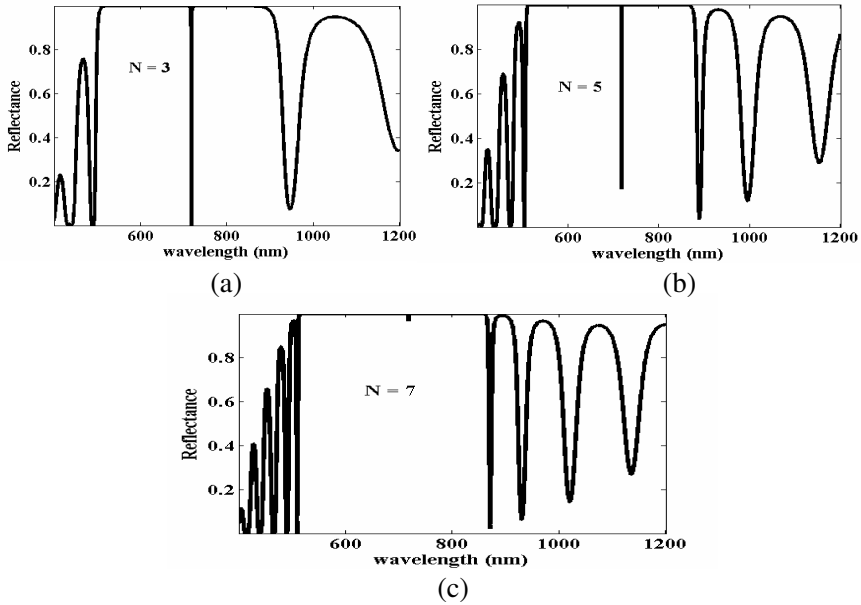


Figure 4. The calculated wavelength-dependant reflectance in 1DTSMDDPC with dielectric defect layer for different $N = 3, 5,$ and $7.$

400 nm and 1200 nm. So, we should take the shorter wavelengths range that is 700 nm to 750 nm to see defect mode clearly. Besides, there are some differences in the sidelobs. By increasing N , fluctuation of

sidelobs increase and the width of PBG is decreased. We see that the resonant peak will appear in 717.5 nm approximately and does not change by increasing of number of periods.

In Figure 5, we show the effect of different refractive indices of dielectric defect layer on the reflectance response. We use $N = 5$, since defect mode will appear clearer in it. Besides, according to the condition $n_d = q\lambda_0/4d_{def}$, where $d_{def} = 120$ nm, $\lambda_0 = 1550$ nm and for different q , the refractive index will be changed. The number of defect modes is increasing by enhancement of q . As we see in Figure 6, there are some differences in sidelobes by increasing the index of refraction of dielectric defect layer. We give the wavelength of the defect modes for different refractive indices in Table 1.

Figure 6 displays the wavelength-dependant reflection for the 1DTSMDPC with different defect layer thicknesses by using condition $d_{def} = q\lambda_0/4n_d$, where $\lambda_0 = 1550$ nm, and $n_d = 3.22$. We see that by increasing the thickness of defect layer, resonant peak will increase. We give the wavelength of the defect modes for different thicknesses in Table 2.

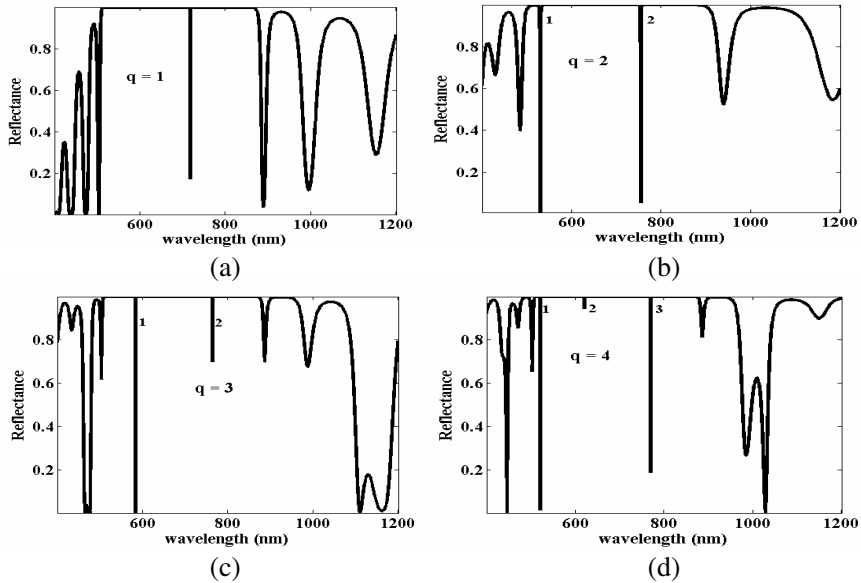


Figure 5. The wavelength-dependant reflectance in 1DTSMDPC at different refractive indices of dielectric defect layer by changing q from 1 to 4. The thickness of defect layer is $d_{def} = 120$ nm, and number of periods is $N = 5$.

Table 1. The number of defect modes and its location for different refractive indices of dielectric defect layer by changing q according to the condition $n_d = q\lambda_0/4d_{def}$.

q	n_d	No. of defect modes	Wavelength (\sim nm)
1	3.22	1	717.5
2	6.45	2	530, 751
3	9.68	2	583, 765
4	12.91	3	521, 620, 769
5	16.14	3	555, 645, 771
6	19.37	4	519, 581, 664, 773
7	22.60	4	544, 603, 678, 773
8	25.83	5	518, 564, 620, 688, 773
9	29.06	5	538, 582, 634, 698, 774
10	32.29	6	518, 554, 596, 646, 704, 774

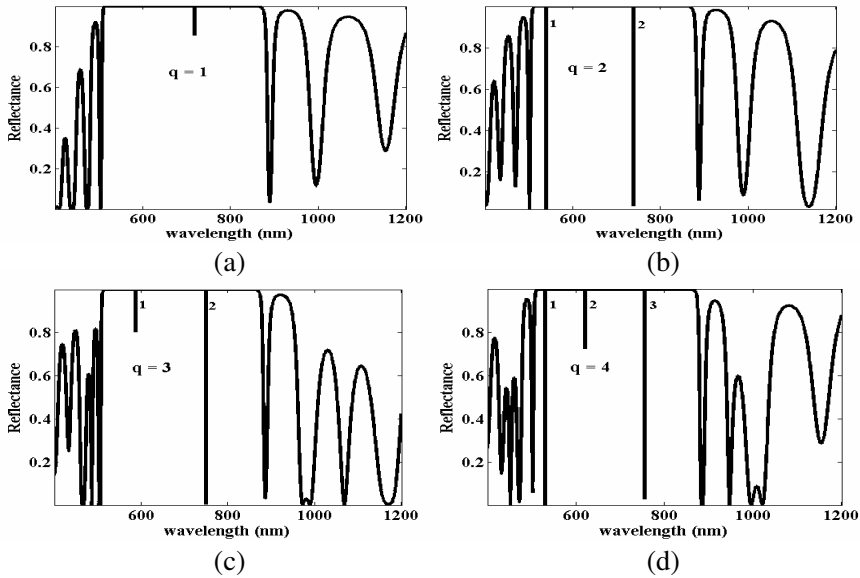


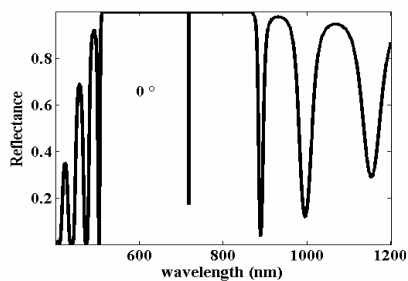
Figure 6. The wavelength-dependent reflectance for 1DTSMDPC at different thicknesses of dielectric defect layer by changing q from 1 to 4.

In Figure 7, we plot the reflectance response for 1DTSMDPC at different angles of incidence at $d_{def} = 120$ nm, $N = 5$, and $q = 1$ for TE wave. We see that resonant peak move to the left (shorter wavelengths)

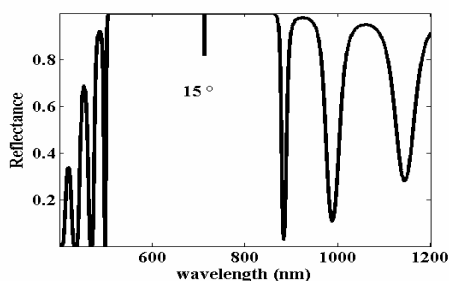
as the angle of incidence increases and in higher angles, the height of resonant peak has decreased in wavelength between 400 nm and 1200 nm. We give the wavelength of the defect modes for different angles of incidence in *TE* wave in Table 3.

Table 2. The number of defect modes and its location for different thicknesses of dielectric defect layer by changing q according to the condition $d_{def} = q\lambda_0/4n_d$.

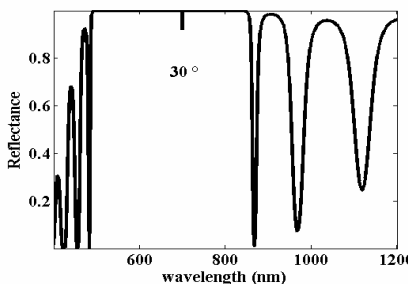
q	d_{def} (\sim nm)	No. of defect modes	Wavelength (\sim nm)
1	120.34	1	717.5
2	240.68	2	539, 739
3	361.02	2	589, 749
4	481.36	3	530, 620, 754
5	601.70	3	560, 642, 759
6	722.04	4	526, 584, 661, 760
7	842.39	4	549, 604, 674, 761
8	962.73	5	524, 568, 620, 685, 763
9	1083.07	5	542, 583, 634, 694, 765
10	1203.41	6	523, 558, 598, 645, 700, 765



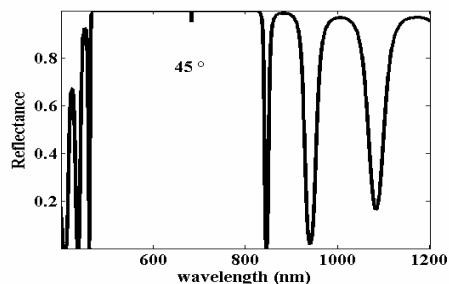
(a)



(b)



(c)



(d)

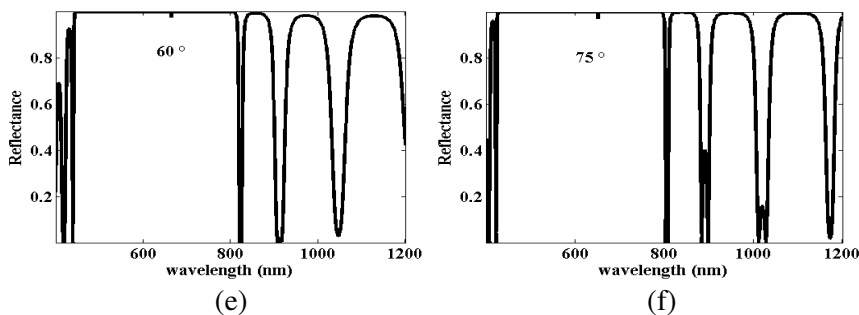


Figure 7. The calculated wavelength-dependant reflectance for the 1DTSM DPC $A/(n_1n_2n_3)^N D(n_3n_2n_1)^N/A$ for TE -wave at different angles of incidence $0^\circ, 15^\circ, 30^\circ, 45^\circ,$ and $60^\circ,$ respectively.

Table 3. The location of dielectric defect layer by changing angle of incidence in TE wave.

Angels in TE wave (degree)	Wavelength (\sim nm)
0°	717.5
15°	713
30°	700
45°	683
60°	665
75°	652

Table 4. The location of dielectric defect layer by changing angle of incidence in TM wave.

Angels in TM wave (degree)	Wavelength (\sim nm)
0°	717.5
15°	713
30°	698
45°	678
60°	654
75°	635

All the above calculations are for TE -wave. Now, in Figure 8, we show wavelength-dependant reflectance of 1DTSM DPC with the structure of $(A/(n_1n_2n_3)^N D(n_3n_2n_1)^N/A)$ for TM -wave at different angles of incidence $0^\circ, 15^\circ, 30^\circ, 45^\circ,$ and $60^\circ,$ respectively. For normal incidence, that is at $0^\circ,$ there is no difference between TE and TM waves. We see that resonant peak move to the left (shorter

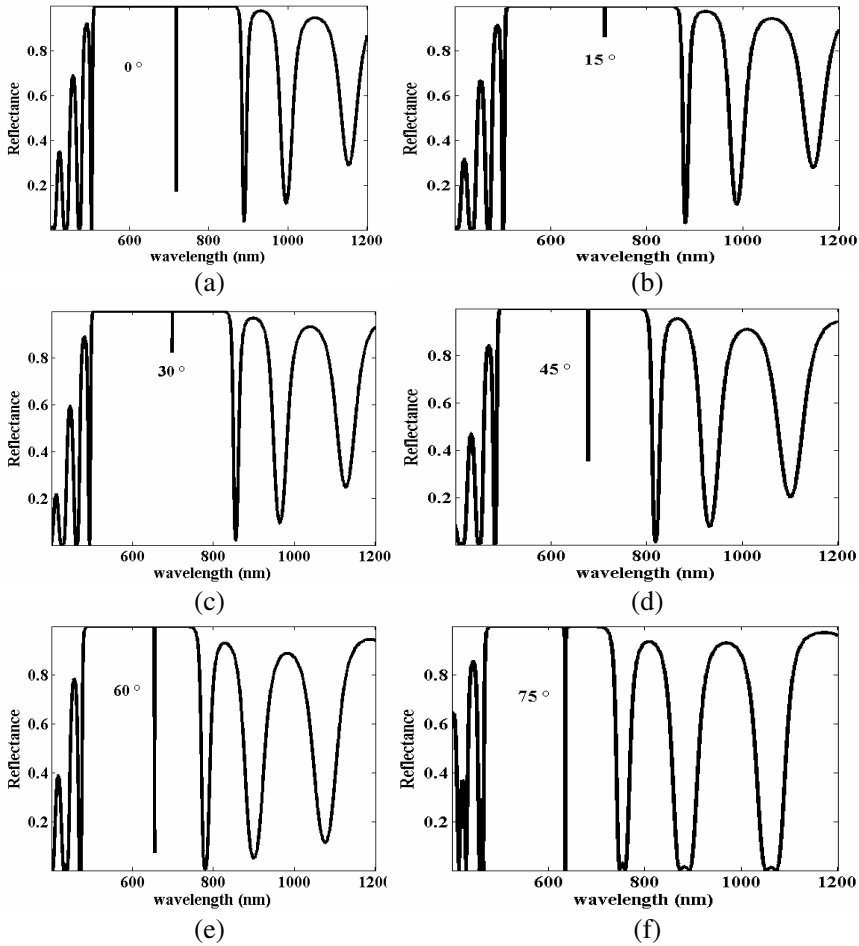


Figure 8. The calculated wavelength-dependant reflectance in 1DTSMDPC for *TM*-wave at different angles of incidence 0° , 15° , 30° , 45° , 60° and 75° , respectively.

wavelengths) as the angle of incidence increases. Besides, the height of resonant peak will change, by changing angle of incidence. We give the wavelength of the defect modes for different angles of incidence in *TM* wave in Table 4.

In all calculations above, we use the structure $A/(n_1n_2n_3)^sD(n_3n_2n_1)^t/A$, in which s and t are equal to 5. Now, we want to change the place of defect mode as depicted in Figure 9. The dependence of peak height on different structures is shown in Figure 9. As can be seen, in Figures 9(a), (b), (c) when the structure is $A/(n_1n_2n_3)^1D(n_3n_2n_1)^9/A$

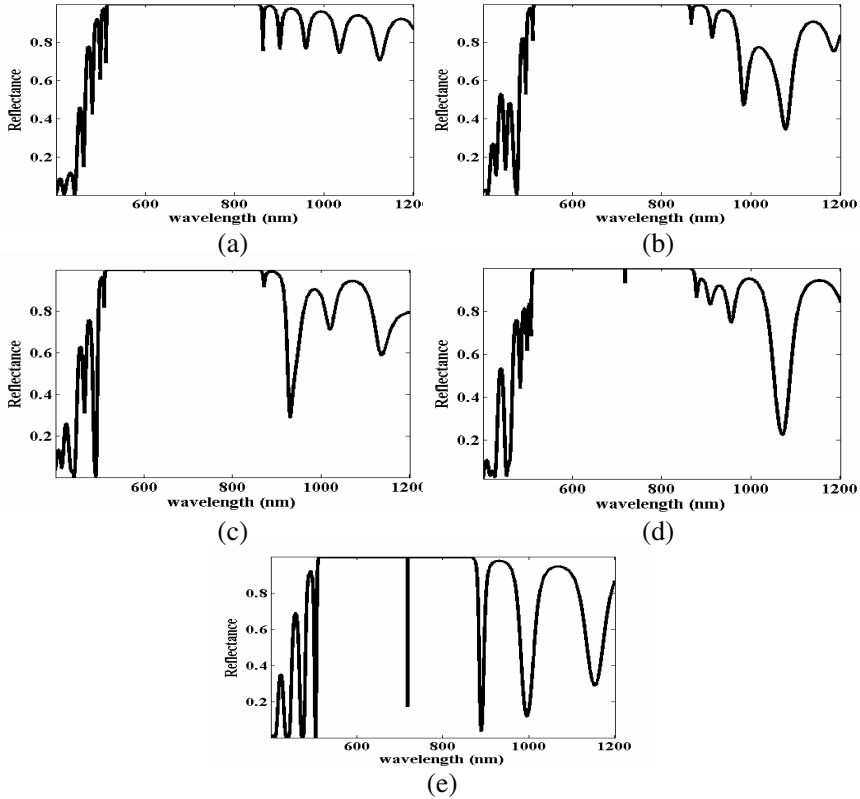


Figure 9. The calculated wavelength-dependant reflectance for 1DTSMDPC in normal incidence at different structures $A/(n_1n_2n_3)^sD(n_3n_2n_1)^t/A$, where (a) $s = 1, t = 9$, (b) $s = 2, t = 8$, (c) $s = 3, t = 7$, (d) $s = 4, t = 6$, (e) $s = 5, t = 5$.

and $A/(n_1n_2n_3)^2D(n_3n_2n_1)^8/A$, there is no defect mode in the BG. But, when the structure $A/(n_1n_2n_3)^4D(n_3n_2n_1)^6/A$, that is near to the complete symmetric, the defect mode will appear but it is incomplete. When the numbers of right and left cells are equal, the resonant peaks are complete. Namely, the values of (s) and (t) are at best to be taken equal for both right and left periods in order to see resonant peak completely (Figure 9(e)).

In this work, we use silver (Ag) as a metal for the second layer. Now, in Figure 10, we use Cu, Ag, and Al with $\omega_p = 2\pi \times 1.914 \times 10^{15}$, $2\pi \times 2.175 \times 10^{15}$, and $2\pi \times 3.570 \times 10^{15}$, respectively [22, 31]. As we can see by increasing ω_p , the location of resonant peak changes to the shorter wavelengths. The wavelengths of defect mode for Cu, Ag,

and Al in Figure 10 are 719 nm, 717.5 nm, 709 nm, respectively. Also, numerical investigations show that BG width is decreased by increasing ω_p .

3.2. Defect Modes with Metallic Defect Layer

All calculations above are done for dielectric defect layer. In Figure 11, we show the effect of using metallic defect layer on the reflectance

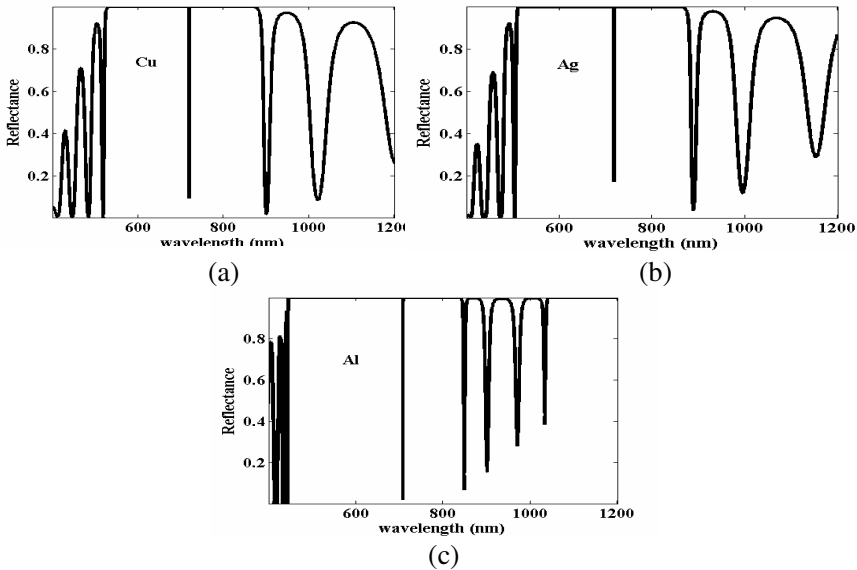


Figure 10. The calculated wavelength-dependant reflectance in 1DTSMDPC with different metals, (a) Cu, (b) Ag, (c) Al.

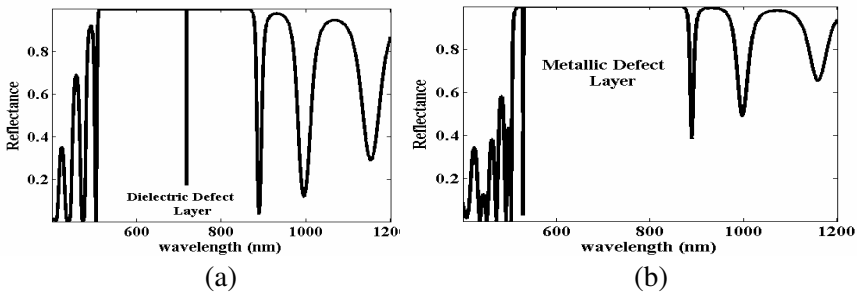


Figure 11. The wavelength-dependant reflectance for 1DTSMDPC using (a) dielectric defect layer with $N = 5$, $d = 120$ nm, (b) metallic defect layer with $d_{def} = 10$ nm.

response as compared with dielectric defect layer for 1DTSMDPC. In normal incidence, we use silver (Ag) defect layer with $N = 5$, $d_{def} = 10$ nm, and $q = 1$. We see that when we use dielectric defect layer, the resonant peak is 717.5 nm, but there is one resonant peak in ~ 529 nm when we use metallic defect layer with thickness of 10 nm. So the resonant peak moves to the shorter wavelengths for metallic defect layer and there are some differences in sidelobes as depicted in Figure 11.

4. CONCLUSION

In this paper, we used TMM and Drude model of metals to calculate PBG of a 1DTSMDPC. We have studied properties of defect modes in defective symmetrical system with structure $A/(n_1n_2n_3)^N D(n_3n_2n_1)^N/A$. As we have shown, there is at least one defect mode in the PBG for dielectric and metallic defect layer, but the number of resonant peaks increases as refractive index and thickness of dielectric defect layer increases. Besides, defect modes move to the shorter wavelengths by increasing the angle of incidence in both TE and TM wave. Moreover, the width of PBG decreases by increasing the number of periods. Also, by increasing ω_p , the location of resonant peak moves to the shorter wavelengths, and numerical investigations show that BG width is decreased by increasing ω_p . Finally, defect mode moves to the shorter wavelengths when we use metallic defect layer, as compared with dielectric one.

ACKNOWLEDGMENT

This work has been financially supported by the Payame Noor University (PNU) I. R. of Iran under the grant No. 1390/3/0/14/185.

REFERENCES

1. Sakoda, K., *Optical Properties of Photonic Crystals*, Springer-Verlag, Berlin, 2001.
2. Joannopoulos, J. D., R. D. Meade, and J. N. Winn, *Photonic Crystals: Molding the Flow of Light*, Princeton University Press, Princeton, NJ, 1995.
3. Dastmalchi, B., R. Kheradmand, A. Hamidipour, A. Mohtashami, K. Hingerl, and J. Zarbakhsh, "Local dispersion of guiding modes in photonic crystal waveguide interfaces and hetero-structures," *Progress In Electromagnetics Research B*, Vol. 26, 39–52, 2010.

4. Noda, S., M. Imada, M. Okano, S. Ogawa, M. Mochizuki, and A. Chutinan, "Semiconductor three-dimensional and two-dimensional photonic crystals and devices," *IEEE J. Quantum Electron.*, Vol. 38, 726–735, 2002.
5. Inoue, K. and K. Ohtaka (eds.), *Photonics Crystals: Physics, Fabrication and Applications*, Springer-Verlag, Berlin, Heidelberg, 2004.
6. Gharaati, A. and Z. Zare, "Photonic band structures and enhancement of omnidirectional reflection bands by using a ternary 1D photonic crystal including left-handed materials," *Progress In Electromagnetic Research M*, Vol. 20, 81–94, 2011.
7. Guida, G., "Numerical studies of disordered photonic," *Progress In Electromagnetics Research*, Vol. 41, 107–131, 2003.
8. Szipocs, R., K. Ferencz, C. Spielmann, and F. Krausz, "Chirped multilayer coatings for broadband dispersion control in femtosecond lasers," *Optics Letters*, Vol. 19, No. 3, 201–203, 1994.
9. Han, P. and H. Z. Wang, "Extension of omnidirectional reflection range in one-dimensional photonic crystals with staggered structure," *J. Opt. Soc. Am. B*, Vol. 20, No. 9, 1996–2001, 2003.
10. Usievich, B. A., A. M. Prokhorov, and V. A. Sychugov, "A photonic-crystal narrow-band optical filter," *Laser Physics*, Vol. 12, No. 5, 898–902, 2002.
11. Chen, D., M.-L. V. Tse, and H.-Y. Tam, "Super-lattice structure photonic crystal fiber," *Progress In Electromagnetic Research M*, Vol. 11, 53–64, 2010.
12. Srivastava, R., K. B. Thapa, S. Pati, and S. P. Ojha, "Omnidirectional reflection in one dimensional photonic crystal," *Progress In Electromagnetics Research B*, Vol. 7, 133–143, 2008.
13. Wang, X., X. Hu, Y. Li, W. Jia, C. Xu, X. Liu, and J. Zi, "Enlargement of omnidirectional total reflection frequency range in one-dimensional photonic crystals by using photonic heterostructures," *Appl. Phys. Lett.*, Vol. 80, 4291–4293, 2002.
14. Fink, Y., J. N. Winn, S. Fan, C. Chen, J. Michel, J. D. Joannopoulos, and L. E. Thomas, "A dielectric omnidirectional reflector," *Science*, Vol. 282, 1679–1682, 1998.
15. Yablonovitch, E., "Inhibited spontaneous emission in solid state physics and electronics," *Phys. Rev. Lett.*, Vol. 58, 2059–2062, 1987.
16. John, S., "Strong localization of photons in certain disordered lattices," *Phys. Rev. Lett.*, Vol. 58, 2486–2489, 1987.
17. Yeh, P., *Optical Waves in Layered Media*, Wiley, New York, 2005.

18. Tang, K., Y. Xiang, and S. Wen, "Tunable transmission and defect mode in one-dimensional ternary left-handed photonic crystal," *Proc. of SPIE*, 60200S.1–60200S.7 (6020), 2005.
19. Skorobogatiy, M. and J. Yang, *Fundamentals of Photonic Crystal Guiding*, 132, Cambridge University Press, 2009.
20. Qi, L.-M. and Z. Yang, "Modified plane wave method analysis of dielectric plasma photonic crystal," *Progress In Electromagnetics Research*, Vol. 91, 319–332, 2009.
21. Jackson, J. D., *Classical Electrodynamics*, 3rd edition, 311–313, California University, 1999.
22. Wu, C.-J., Y.-H. Chung, B.-J. Syu, and T.-J. Yang, "Band gap extension in a one-dimensional ternary metal-dielectric photonic crystal," *Progress In Electromagnetics Research*, Vol. 102, 81–93, 2010.
23. Srivastava, R., S. Srivastava, and S. P. Ojha, "Negative reflection by photonic crystal," *Progress In Electromagnetics Research B*, Vol. 2, 15–26, 2008.
24. Topasna, D. M. and G. A. Topasna, "Numerical modeling of thin film optical filters," *J. Opt. Soc. Am. A*, 2009.
25. Awasthi, S. K., U. Malaviya, and S. P. Ojha, "Enhancement of omnidirectional total-reflection wavelength ranges by using one-dimensional ternary photonic bandgap material," *J. Opt. Soc. Am. B: Optical Physics*, Vol. 23, 2566–2571, 2006.
26. Awasthi, S. K. and S. P. Ojha, "Design of a tunable optical filter by using a one-dimensional ternary photonic band gap material," *Progress In Electromagnetics Research M*, Vol. 4, 117–132, 2008.
27. Born, M. and E. Wolf, *Principles of Optics*, Cambridge, London, 1999.
28. Saleh, B. E. A. and M. C. Teich, *Fundamentals of Photonics*, 244, Wiley, New York, 2007.
29. Orfanidis, S. J., *Electromagnetic Waves and Antennas*, Rutgers University, 2008, www.ece.rutgers.edu/orfanidi/ewa.
30. Markos, P. and C. M. Soukoulis, *Wave Propagation: From Electrons to Photonic Crystals and Left Handed Materials*, Princeton University Press, New Jersey, 2008.
31. Marquez-Islas, R., B. Flores-Desirena, and F. Perez-Rodriguez, "Exciton polaritons in one dimensional metal-semiconductor photonic crystal," *J. Nanosci. Nanotechnol.*, Vol. 8, 6584–6588, 2008.